








Reverse Genetics System for Heartland Bandavirus: NSs Protein Contributes to Heartland Bandavirus Virulence

 Satoshi Taniguchi,^a Takuya Inagaki,^a Shigeru Tajima,^a Tadaki Suzuki,^b  Tomoki Yoshikawa,^a Shuetsu Fukushi,^a Eun-Sil Park,^c Hikaru Fujii,^d Shigeru Morikawa,^d  Hideki Tani,^e Eri Nakayama,^a Takahiro Maeki,^a Masayuki Shimojima,^a  Chang-Kweng Lim,^a  Masayuki Saijo^a

^aDepartment of Virology I, National Institute of Infectious Diseases, Tokyo, Japan

^bDepartment of Pathology, National Institute of Infectious Diseases, Tokyo, Japan

^cDepartment of Veterinary Science, National Institute of Infectious Diseases, Tokyo, Japan

^dFaculty of Veterinary Medicine, Okayama University of Science, Ehime, Japan

^eDepartment of Virology, Toyama Institute of Health, Toyama, Japan

ABSTRACT Heartland bandavirus (HRTV), which is an emerging tick-borne virus first identified in Missouri in 2009, causes fever, fatigue, decreased appetite, headache, nausea, diarrhea, and muscle or joint pain in humans. HRTV is genetically close to Dabie bandavirus, which is the causative agent of severe fever with thrombocytopenia syndrome (SFTS) in humans and is known as SFTS virus (SFTSV). The generation of infectious HRTV entirely from cloned cDNAs has not yet been reported. The absence of a reverse genetics system for HRTV has delayed efforts to understand its pathogenesis and to generate vaccines and antiviral drugs. Here, we developed a reverse genetics system for HRTV, which employs an RNA polymerase I-mediated expression system. A recombinant nonstructural protein (NSs)-knockout HRTV (rHRTV-NSsKO) was generated. We found that NSs interrupted signaling associated with innate immunity in HRTV-infected cells. The rHRTV-NSsKO was highly attenuated, indicated by the apparent absence of symptoms in a mouse model of HRTV infection. Moreover, mice immunized with rHRTV-NSsKO survived a lethal dose of HRTV. These findings suggest that NSs is a virulence factor of HRTV and that rHRTV-NSsKO could be a vaccine candidate for HRTV.

IMPORTANCE Heartland bandavirus (HRTV) is a tick-borne virus identified in the United States in 2009. HRTV causes fever, fatigue, decreased appetite, headache, nausea, diarrhea, and muscle or joint pain in humans. FDA-approved vaccines and antiviral drugs are unavailable. The lack of a reverse genetics system hampers efforts to develop such antiviral therapeutics. Here, we developed a reverse genetics system for HRTV that led to the generation of a recombinant nonstructural protein (NSs)-knockout HRTV (rHRTV-NSsKO). We found that NSs interrupted signaling associated with innate immunity in HRTV-infected cells. Furthermore, rHRTV-NSsKO was highly attenuated and immunogenic in a mouse model. These findings suggest that NSs is a virulence factor of HRTV and that rHRTV-NSsKO could be a vaccine candidate for HRTV.

KEYWORDS Heartland bandavirus, reverse genetics, vaccine, NSs protein

The emerging tick-borne bunyavirus Heartland bandavirus (HRTV) causes Heartland bandavirus disease in humans (1). HRTV was first isolated in 2009 from two farmers in Missouri who were hospitalized with severe fever, leukopenia, and thrombocytopenia (2). Subsequently, as of January 2021, more than 50 cases of HRTV disease, including fatalities, occurred in Arkansas, Georgia, Illinois, Indiana, Iowa, Kansas, Kentucky, Missouri, North Carolina, Oklahoma, and Tennessee (3). Evidence implicates the Lone Star tick (*Amblyomma americanum*) as the main vector that transmits the virus during multiple stages of its life cycle to hosts such as white-tailed deer, horses, raccoons,

Editor Rebecca Ellis Dutch, University of Kentucky College of Medicine

Copyright © 2022 American Society for Microbiology. All Rights Reserved.

Address correspondence to Satoshi Taniguchi, rei-tani@nih.go.jp, or Masayuki Saijo, msaijo@nih.go.jp.

The authors declare no conflict of interest.

Received 18 January 2022

Accepted 26 February 2022

Published 23 March 2022

opossums, and dogs (1, 4, 5). Recently, viral RNA was detected in a Lone Star tick, which was removed from a resident of Suffolk County, New York (6).

HRTV belongs to the genus *Bandavirus*, family *Phenuiviridae*, order *Bunyvirales* (7). *Bandavirus* comprises seven species, including human-pathogenic viruses such as *Bhanja bandavirus* (BHAV) and *Dabie bandavirus*. Dabie bandavirus is generally called severe fever with thrombocytopenia syndrome virus (SFTSV), a causative agent of severe fever with thrombocytopenia syndrome (SFTS) in China, Japan, South Korea, Vietnam, and Taiwan (8–13). In contrast, HRTV is a unique human pathogen in the United States (1).

The HRTV genome comprises one ambisense and two negative-sense single-stranded RNA segments designated S, M, and L (1). The S segment (approximately 1.8 kilobases [kb]) encodes a nonstructural protein (NSs) and a nucleocapsid (N) protein. This segment utilizes an ambisense coding strategy in which the two open reading frames are encoded in opposite transcriptional orientations, terminating in a central intergenic region. The M and L segments (3.4 kb and 6.4 kb, respectively) encode a polyprotein precursor (GPC) that is cleaved into the glycoproteins Gn and Gc, as well as an RNA-dependent RNA polymerase (L protein), respectively. N and L proteins are required for the transcription of the viral genome and viral RNA replication (14). Gn/Gc mediate viral entry into cells and incorporate the ribonucleoprotein complex into the virus particle (15). Studies of NSs expression *in vitro* suggest that the NSs of HRTV functions as an interferon (IFN) antagonist, as well as in SFTSV and the other bunyaviruses (16–20). However, their functions in authentic HRTV *in vitro* and *in vivo* are unknown because of the absence of a suitable reverse genetics system.

Vaccines and drugs against HRTV remain to be developed. Reverse genetics systems are required to introduce mutations into the viral genome arbitrarily and develop antiviral strategies. A reverse genetics system for SFTSV has been reported, and the system employs T7 RNA polymerase (21). Here, we established polymerase I-driven reverse genetics systems for HRTV. Furthermore, we attempted to introduce mutations into the open reading frame (ORF) of the NSs and assessed the role of NSs as well as the pathogenicity and potency of the generated recombinant NSs protein-knockout viruses as a vaccine.

RESULTS

Nucleotide sequence of the HRTV genome. To generate a recombinant virus genetically identical to authentic wild-type (wt) HRTV, the complete genome sequence of HRTV strain MO-4-National Institute of Infectious Diseases (NIID) was determined (GenBank accession numbers [LC629153](#), [LC629154](#), and [LC629155](#)). The 5'- and 3'-terminal nucleotide sequences of the S, M, and L segments were determined (Fig. 1A). One nucleotide (cytosine) in the S segment of the 5'-untranslated region (UTR) differed from other nucleotide sequences of the S segment (GenBank accession numbers [JX005842](#), [JX005843](#), and [KJ740146](#)). HRTV strain MO-4-NIID was further propagated in Vero 9013 cells, was designated wtHRTV, and was used in this study. The genomic sequence differences between HRTV strain MO-4-NIID and wtHRTV are shown in Table 1 and Fig. 1B. Several nucleotide substitutions were identified in the L segment.

Development of HRTV minigenome assays. Minigenome assays were developed to assess the transcriptional and replicational functionalities of ribonucleoproteins generated using an RNA polymerase I-mediated expression system and recombinant N and L proteins. Polymerase I-driven pRF vector-based M segment minigenome plasmids (HRTV-MMG), T7-driven N and L expression plasmids (pTM1-HRTV-N and pTM1-HRTV-L), and polymerase-II-driven N and L expression plasmids (pKS-HRTV-N and pKS-HRTV-L) were constructed, and minigenome assays were performed using BSR-T7/5 cells (Fig. 2A). The expression of NanoLuc 1.1 luciferase (Nluc) was significantly high in BSR-T7/5 cells when they were cotransfected with HRTV-MMG and both N and L expression T7 polymerase-driven plasmids (Fig. 2B). In addition, Nluc expression was detected in BSR-T7/5 cells when N and L were expressed, independent of T7 polymerase or polymerase II (Fig. 2C).

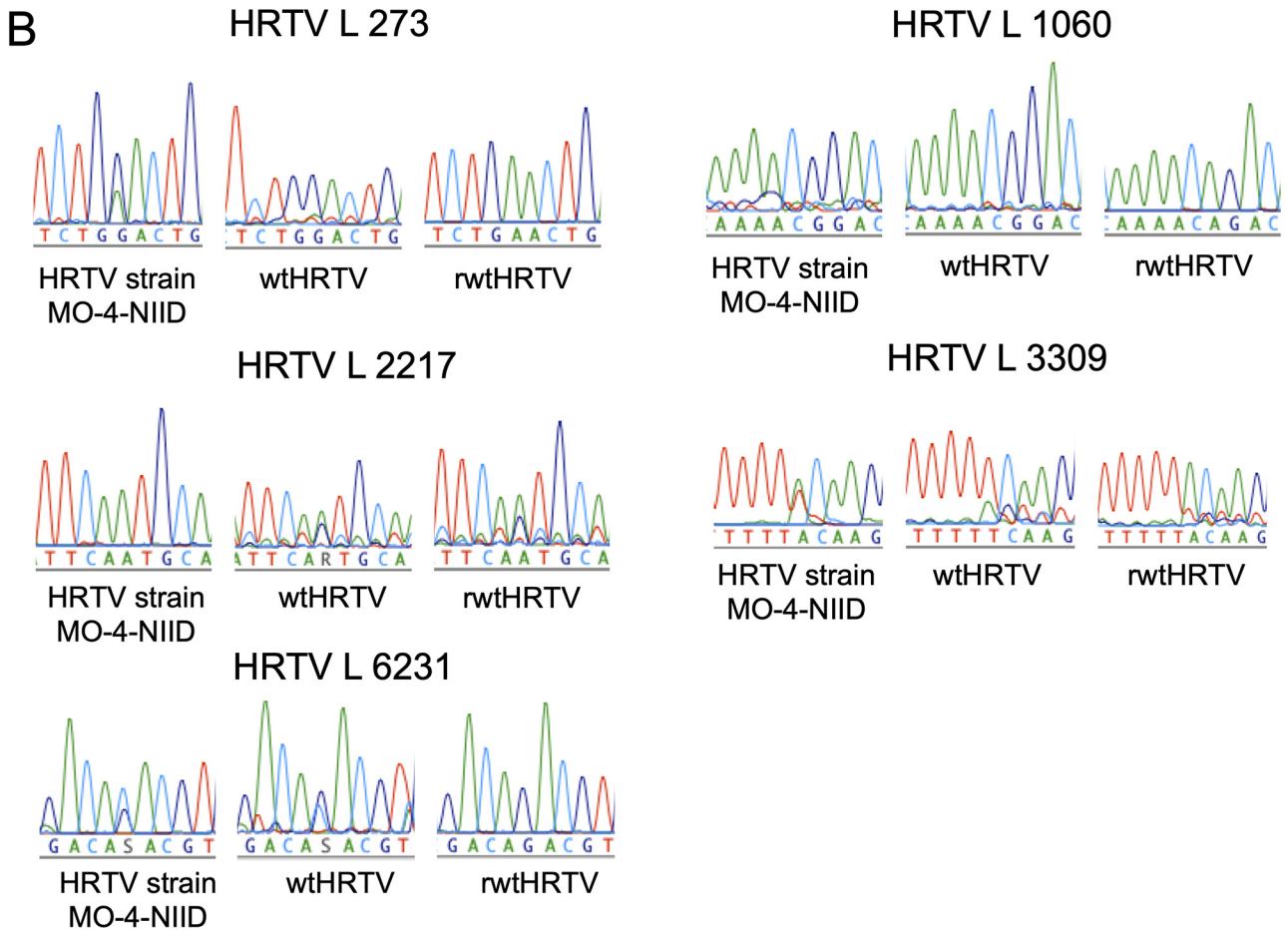
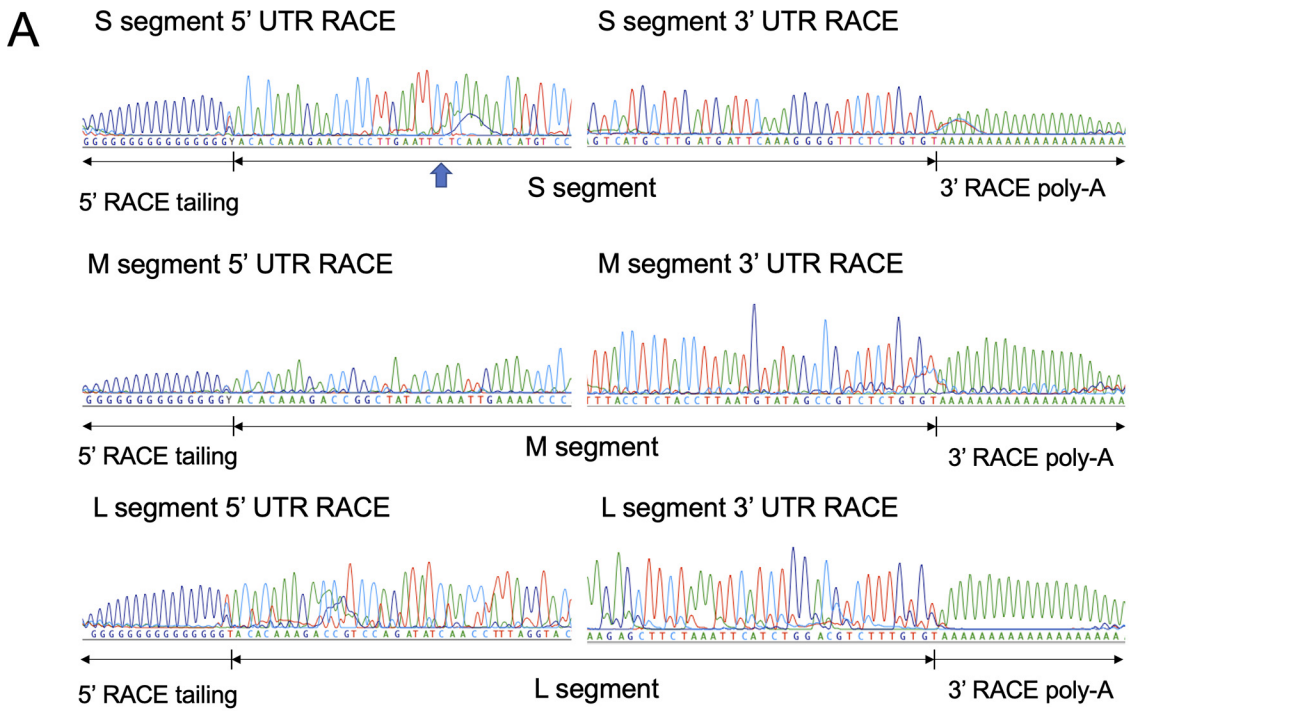


FIG 1 Determination of the HRTV genome sequence and comparison of viral genome sequences. (A) Determination of the terminal nucleotide sequences of HRTV S, M, and L segments. Cytosine is indicated using the blue arrow at the S segment's 5' UTR to show which base differed from other HRTV S segment nucleotide sequences deposited in GenBank. (B) Sequencing electropherograms at nucleotide positions 273, 1060, 2217, 3309, and 6231 at the L segment of HRTVs (cRNA orientation).

TABLE 1 Nucleic acid differences of viral genome sequences of HRTVs

Segment	Nucleotide position (cRNA orientation)	Nucleotide difference by strain ^a				Amino acid change
		HRTV-MO-4-NIID	wtHRTV	pRF-HRTV-L	rwHRTV	
L	273	G/A	G	A	A	G86E
L	1060	G	G	A	A	Synonymous
L	2217	A	A/G	A	A/G	N734S
L	3309	A/T	T/A	A	A	Y1098F
L	6231	C/G	G/C	G	G	T2072R

^aSequences represented by "x/y" indicate that the nucleic acid sequence of this nucleotide position was a mixture of "x" and "y" and the major nucleic acid was "x."

Generation of recombinant HRTV. Polymerase I-driven pRF vector-based HRTV-S, M, and L RNA-segment expression plasmids were constructed (pRF-HRTV-S, pRF-HRTV-M, and pRF-HRTV-L, respectively). As observed, the pRF-HRTV-L plasmid contained two nonsynonymous substitutions and one synonymous substitution in the L protein ORF (Table 1). These substitutions were located at the 273rd, 1,060th, and 6,231st nucleotide in the cRNA orientation of the L segment, respectively. Particularly, the 273rd and 6,231st nonsynonymous substitutions were identified in the viral sequence of HRTV-MO-4-NIID, which were considered nonartificial substitutions (Table 1 and Fig. 1B). Reverse genetics assays were performed using BSR-T7/5 cells transfected with these plasmids and the N and L expression plasmids used in minigenome assays (pTM1-HRTV-N, pTM1-HRTV-L, pKS-HRTV-N, and pKS-HRTV-L) (Fig. 3A). Viral replication was observed only when L was supplied by the T7-driven plasmid (Table 2). However, virus rescue was observed when N was supplied with the T7-driven and polymerase-II-driven plasmids. The complete genome sequences of the rescued recombinant HRTV (rwHRTV) revealed a nucleotide sequence change encoding predicted a nonsynonymous amino acid residue substitution (N734S) in the L protein of the rwHRTV L segment (Table 1 and Fig. 1B). Nevertheless, this nucleic difference was detected in the electropherograms of the wtHRTV sequence, which were considered naturally obtained through the passages in Vero 9013 cells. The replication kinetics of rwHRTV in Vero 9013 cells compared with those of authentic virus (wtHRTV) are shown in Fig. 3B. The virus titer of rwHRTV was slightly higher than that of wtHRTV at 24 and 48 h after infection. However, virus titers were similar at other times.

Generation and characterization of NSs gene-knockout HRTV. To investigate the function of HRTV NSs, an NSs gene-knockout HRTV (rHRTV-NSsKO) was generated using pRF-HRTV-S-mutaNSs, which harbors mutations in the NSs ORF (Fig. 4A and B). The plaque morphology of rHRTV-NSsKO was unclear compared with that of rwHRTV (Fig. 4C). The growth efficiency of rHRTV-NSsKO in Vero 9013 cells was significantly lower than that of rwHRTV (Fig. 4D). The maximum titer of rwHRTV in Vero 9013 cells was approximately 2.1×10^7 focus-forming units (FFU)/mL, whereas that of rHRTV-NSsKO was approximately 1.1×10^5 FFU/mL. The growth efficiency of rHRTV-NSsKO in A549 cells was significantly lower than that of rwHRTV (Fig. 4E). The maximum virus yields of rHRTV-NSsKO in A549 cells were approximately 2.3×10^3 FFU/mL and was 1.9×10^3 -fold lower than that of rwHRTV.

Suppression of type I-IFN signaling by HRTV NSs. The levels of the mRNAs encoding type I-IFN signaling-related proteins in A549 cells infected with rwHRTV or rHRTV-NSsKO are shown in Fig. 4F to J. The levels of IFN- β mRNA associated with rHRTV-NSsKO infection were significantly higher than those of rwHRTV (Fig. 4F). Furthermore, the mRNA levels of IFN-stimulated genes (ISGs), such as hISG15 and MxA of rHRTV-NSsKO-infected cells, were significantly higher than those of rwHRTV (Fig. 4G and H). Moreover, in infected cells, the mRNA levels of pattern recognition receptors, such as retinoic acid-inducible protein I (RIG-I) and Toll-like receptors 3 (TLR3) of rHRTV-NSsKO, were significantly higher than those of rwHRTV (Fig. 4I and J). There were no significant differences in the cells between the levels of mRNAs encoding IFN- β , hISG15, MxA, RIG-I, and TLR3 of rwHRTV-infected and mock-infected A549 cells (Fig. 4F to J).

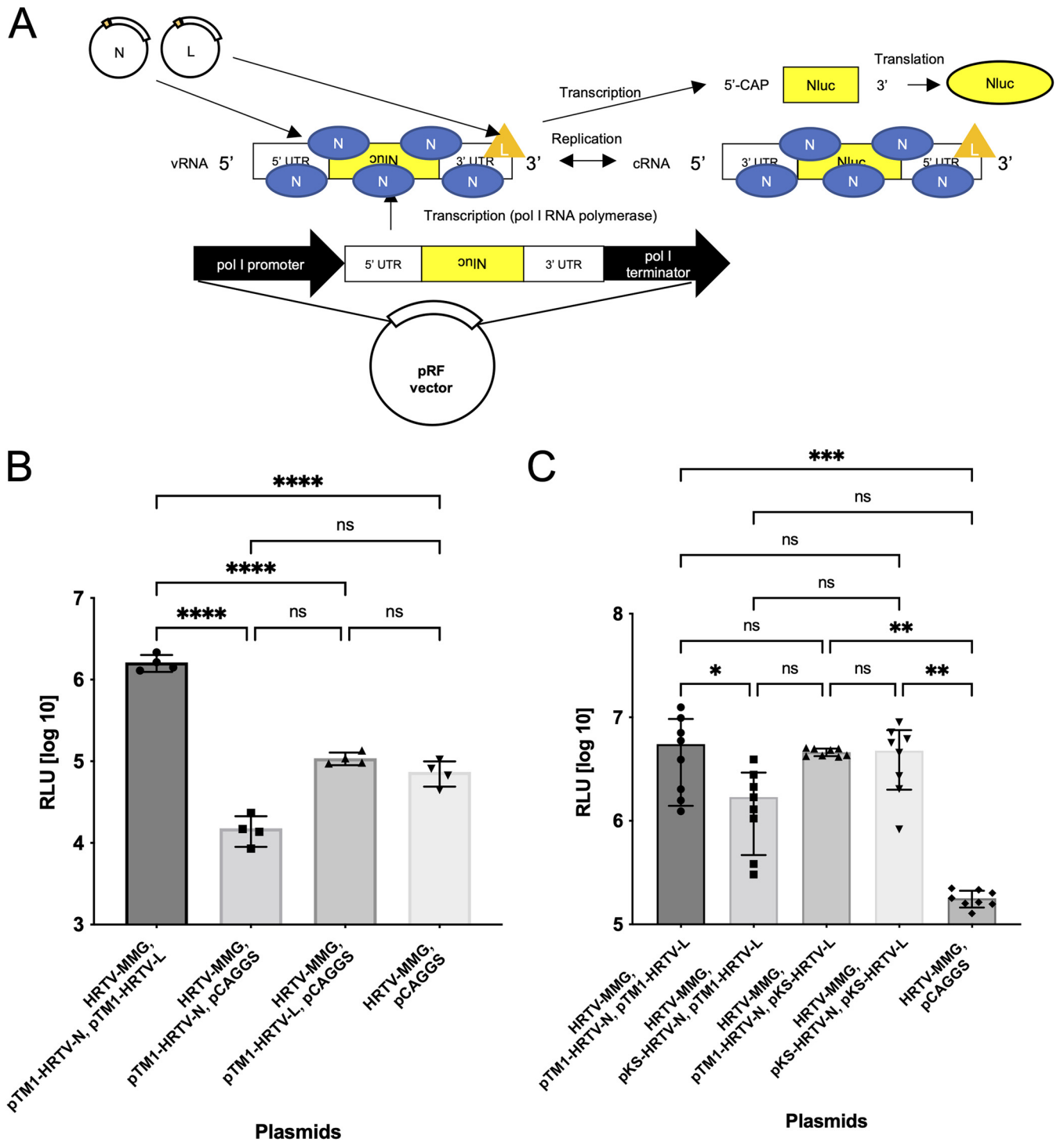


FIG 2 Development of murine polymerase I-mediated HRTV minigenome system. (A) A diagram of the HRTV M segment minigenome plasmid (HRTV-MMG) and its replication, transcription, and translation mechanisms. A cDNA fragment containing the M 3' UTR, Nluc ORF, and the M 5' UTR in the genomic sense is inserted between the murine pol I promoter and the terminator of a pRF vector. The MMG plasmid is transcribed using RNA polymerase I to generate vRNA in BSRT7/5 cells. The vRNAs are then encapsidated with the N protein. The cRNAs are produced in the presence of the L protein. The encapsidated vRNA is transcribed into a reporter-gene mRNA. Finally, the transcribed mRNA is translated by the host to produce Nluc. (B) An HRTV minigenome system was established. BSRT7/5 cells were transfected with HRTV-MMG and pTM1-HRTV-N or pCAGGS, pTM1-HRTV-L or pCAGGS, and pT7-Fluc. Transfected cells were incubated for 2 days at 37°C. Nluc and Fluc activities were measured, and the RLU of luciferase were determined. (C) BSRT7/5 cells were transfected with HRTV-MMG, and pTM1-HRTV-N or pKS-HRTV-N, pTM1-HRTV-L or pKS-HRTV-L, and pT7-Fluc. Control cells were transfected with HRTV-MMG, pCAGGS, and pT7-Fluc. Transfected cells were incubated for 2 days at 37°C. Nluc and Fluc activities were measured, and the RLU of luciferase were determined. Error bars represent the SD. ****, $P < 0.0001$; ***, $P < 0.001$; **, $P < 0.01$; *, $P \leq 0.05$; ns, $P > 0.05$. Experiments shown in panels B and C were performed in quadruplicate and octuplicate, respectively.

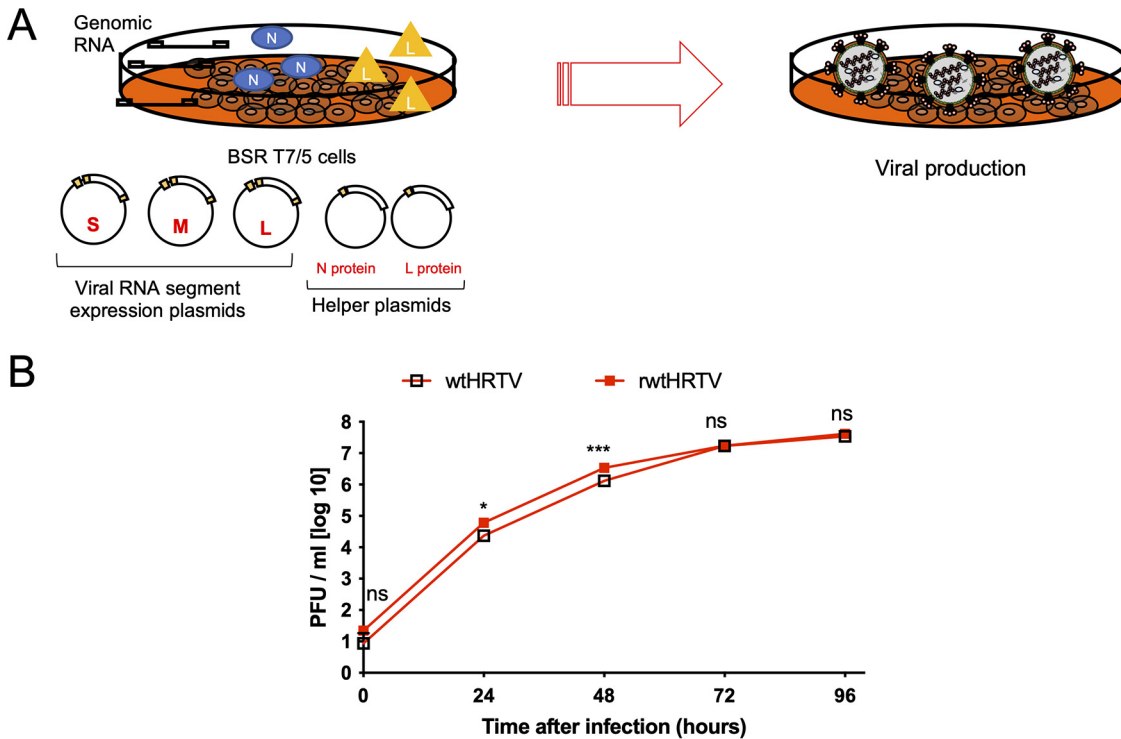


FIG 3 Development of murine polymerase I-mediated HRTV reverse genetics system. (A) Diagram of the production of HRTV using a reverse genetics system. BSR T7/5 cells were transfected with murine polymerase I-driven plasmids to generate S, M, and L viral genomes and helper plasmids to supply viral N and L proteins to the cells. Recombinant viruses were generated in BSR T7/5 cells. (B) Comparison of replication kinetics of wtHRTV and rwtHRTV in Vero 9013 cells. Results are expressed as the mean viral titer of triplicate experiments. Error bars denote the SD. *******, $P < 0.001$; *****, $P < 0.05$; **ns**, $P > 0.05$. Experiments shown in B were performed in triplicate wells for each condition and repeated three times.

The IFN- β -driven activation level of the interferon-sensitive response element (ISRE) promoter was assessed in rwtHRTV and rHRTV-NSsKO-infected 293T cells. The results showed that the inhibition of the IFN- β -driven activation of the ISRE promoter was reduced significantly by knocking out the NSs gene of HRTV (Fig. 4K). We also assessed how the IFN- β -driven ISRE activation was suppressed in NSs-expressing 293T cells. A transient expression of NSs in HRTV inhibited the IFN- β -driven activation of the ISRE promoter in the 293T cells (Fig. 4L and M).

Tissue distribution and pathogenicity of rHRTV-NSsKO in AG129 mice. The tissue distribution and pathogenicity of rHRTV-NSsKO in AG129 mice at 7 days postinfection (dpi) were compared with those of rwtHRTV. Virus genome RNA copy numbers in the plasma, spleen, liver, intestine, and kidney of rHRTV-NSsKO-infected mice were significantly lower than those of rwtHRTV-infected mice (Fig. 5A and B). The spleen, liver, intestine, and kidney of mice inoculated with rwtHRTV, rHRTV-NSsKO, or medium were subjected to histopathological and immunohistochemical analyses. The spleens of rwtHRTV-infected mice exhibited neutrophilic infiltration with obvious nuclear debris and numerous viral antigen-positive cells. In contrast, these pathological changes and HRTV-positive cells were not observed in the spleens of rHRTV-NSsKO-infected and mock mice (Fig. 5C). The livers and kidneys of rwtHRTV- but not rHRTV-NSsKO-infected mice exhibited neutrophilic infiltration and viral antigen-positive cells (Fig. 5D and E).

TABLE 2 Combinations of helper plasmids and viral rescue or not

N expression plasmid	L expression plasmid	Recombinant virus
pTM1-HRTV-N	pTM1-HRTV-L	Rescued
pTM1-HRTV-N	pKS-HRTV-L	Not rescued
pKS-HRTV-N	pTM1-HRTV-L	Rescued
pKS-HRTV-N	pKS-HRTV-L	Not rescued

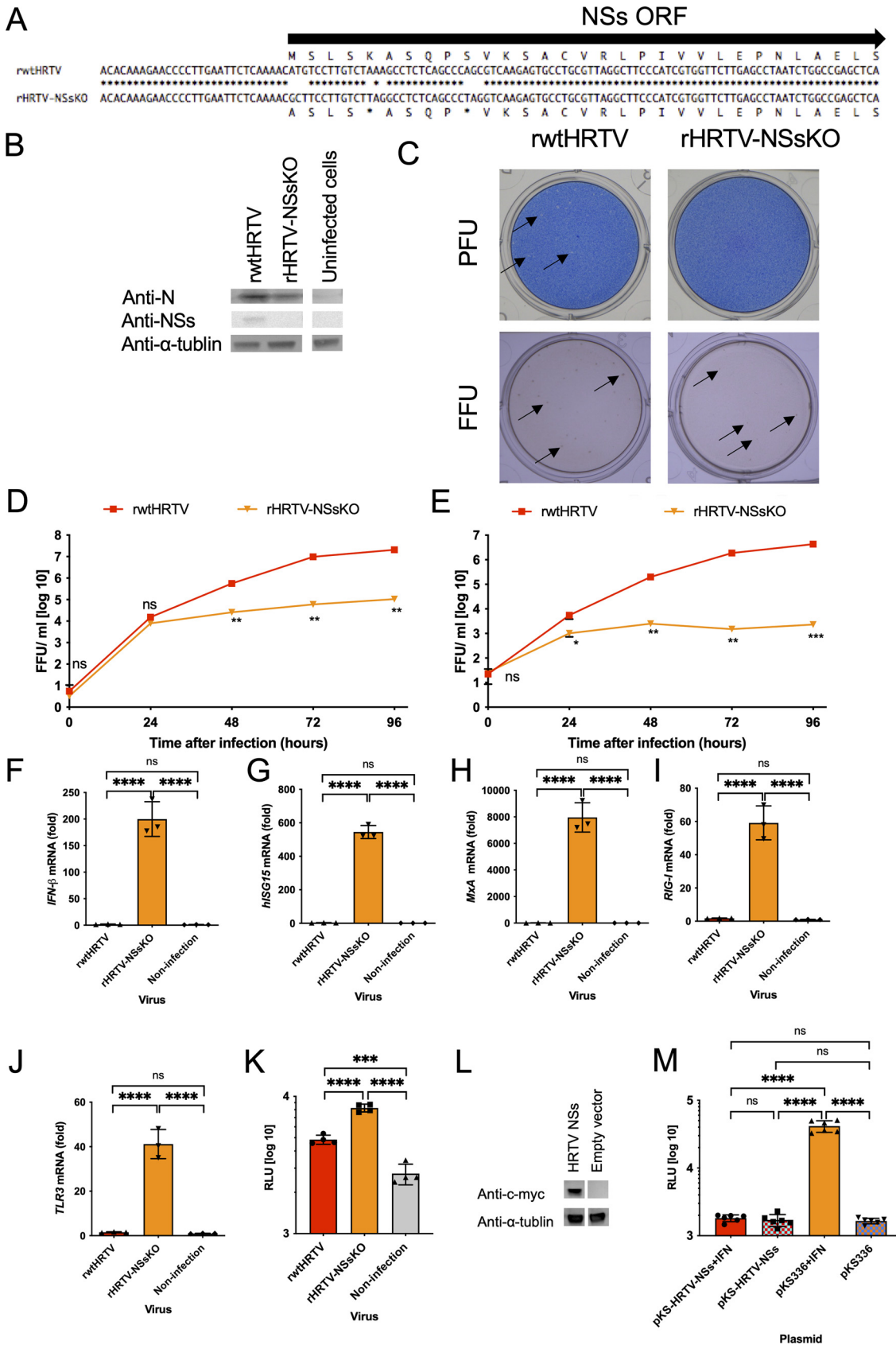


FIG 4 An analysis of the function of HRTV NSs in type I interferon-mediated innate immunity. (A) Alignment of the genomic sense S RNA coding sequences of rwHRTV and rHRTV-NSsKO. The methionine at the translation initiation codon of the NSs (Continued on next page)

Virulence of rHRTV-NSsKO in AG129 mice and its potency as a live-attenuated vaccine against HRTV. AG129 mice were infected subcutaneously (s.c.) with 1.0×10^2 FFU of rwtHRTV, rHRTV-NSsKO, or medium ($n = 10$ per group) (Fig. 6A). All mice infected with rwtHRTV died within 10 days post-first infection (dpfi), whereas all mice infected with rHRTV-NSsKO survived (Fig. 6B). Mice infected with rHRTV-NSsKO suffered no apparent weight loss (Fig. 6C).

Half of the mice infected with rHRTV-NSsKO or medium were further infected with 1.0×10^2 FFU of rwtHRTV on 35 dpfi (rHRTV-NSsKO_rwtHRTV and medium_rwtHRTV; $n = 5$ per group) (Fig. 6A). All rHRTV-NSsKO_rwtHRTV mice survived the second infection; however, all medium_rwtHRTV mice died after the second infection (Fig. 6D and E).

Neutralization titers against HRTV of plasma collected from mice on -1 dpfi, -1 days post-second infection (dpsi), and 14 dpsi are shown in Fig. 6F. Anti-HRTV neutralizing antibodies were detected in all rHRTV-NSsKO_rwtHRTV mice on -1 dpsi and 14 dpsi. HRTV RNA was detected in all plasma collected from mice first inoculated with medium and then inoculated with rwtHRTV (medium_rwtHRTV) on 5 dpsi, whereas the plasma of 4 of 5 rHRTV-NSsKO_rwtHRTV mice were negative for HRTV RNA on 5 dpsi (Fig. 6G). Viral RNA was not detected in all plasma collected 2 dpsi.

DISCUSSION

Here, we describe the development of reverse genetics systems for HRTV to generate the NSs gene knockout designated rHRTV-NSsKO. The molecular genetic tool contributed new insights into the role of NSs, the pathogenesis of HRTV, and strategies to develop an HRTV vaccine.

The complete genome sequences of each HRTV strain MO-4-NIID segment revealed that a cytosine residue in the S segment of the 5' UTR differed from those of other HRTV-S segment nucleotide sequences deposited in GenBank (Fig. 1A). This cytosine was located at the 22nd nucleotide from the 5' terminus and was considered not to affect viral transcription and replication efficiency. The sequence differences between the HRTV strain MO-4-NIID and wtHRTV were also proposed to be acquired during viral passage in Vero 9013 cells (Fig. 1B and Table 1).

According to published techniques (21–24), we tried to generate a T7 RNA polymerase-driven HRTV reverse genetics system. However, expression constructs of the T7 RNA polymerase-driven M and L segments failed because of unexpected mutations or deletions during plasmid propagation in *Escherichia coli*. Thus, all viral RNAs synthesized here were transcribed by RNA polymerase I. Next, we generated an RNA polymerase I-driven M segment minigenome system (Fig. 2), in which the N and L proteins were expressed by T7 RNA polymerase-driven plasmids (Fig. 2B). The minigenome assay demonstrated that the N and L proteins were essential for viral genome transcription and replication. The reporter protein (Nluc) was coexpressed with N and L, independently of whether these proteins were supplied by the T7 RNA polymerase or RNA polymerase II (Fig. 2C). However, we did not detect virus production if the L protein was supplied by an RNA polymerase-II-driven L expression plasmid (pKS-HRTV-L)

FIG 4 Legend (Continued)

protein was substituted with alanine, and two stop codons were inserted into the NSs protein ORF. (B) Vero 9013 cells were infected at an MOI of 0.1 FFU/cell with recombinant viruses. On 3 days postinfection (dpi), cell lysates were immunoblotted to detect the indicated proteins. (C) Shown is a comparison of plaque and focus morphologies of rwtHRTV and rHRTV-NSsKO. Plaques and focuses are pointed out by arrows. Shown are comparisons of replication kinetics of rwtHRTV and rHRTV-NSsKO in Vero 9013 cells (D) and A549 cells (E). Shown are the IFN- β (F), human ISG15 (G), MxA (H), RIG-I (I), and TLR3 (J) mRNA levels in A549 cells infected with each recombinant virus. (K) Activation levels of the ISRE promoter in 293T cells infected with each recombinant virus at an MOI of 2. 293T cells were transfected with pISRE-TA-luc or pTA-luc and pRL-TK. First, the cells were incubated for 15 h at 37°C and then inoculated with recombinant viruses. After 48 h, the activities of Fluc and Rluc were measured. (L) Expression of recombinant NSs proteins in 293T cells. (M) Activation levels of the ISRE promoter in 293T cells, which transiently expressed recombinant NSs protein and were stimulated with IFN- β . 293T cells were transfected with pISRE-TA-luc or pTA-luc, pRL-TK, and pKS-HRTV-NSs-c-myc or pKS336 (empty vector cells). First, the cells were incubated for 48 h and then treated with IFN- β . After 18 h, the activities of Fluc and Rluc were measured. Error bars represent the SD. ****, $P < 0.0001$; ***, $P < 0.001$; ns, $P > 0.05$. Experiments shown in D and E were performed in triplicate wells for each condition and repeated three times. Experiments shown in F, G, H, I, and J were performed three times. Experiments shown in K and M were performed in quadruplicate and sextuplicate, respectively.

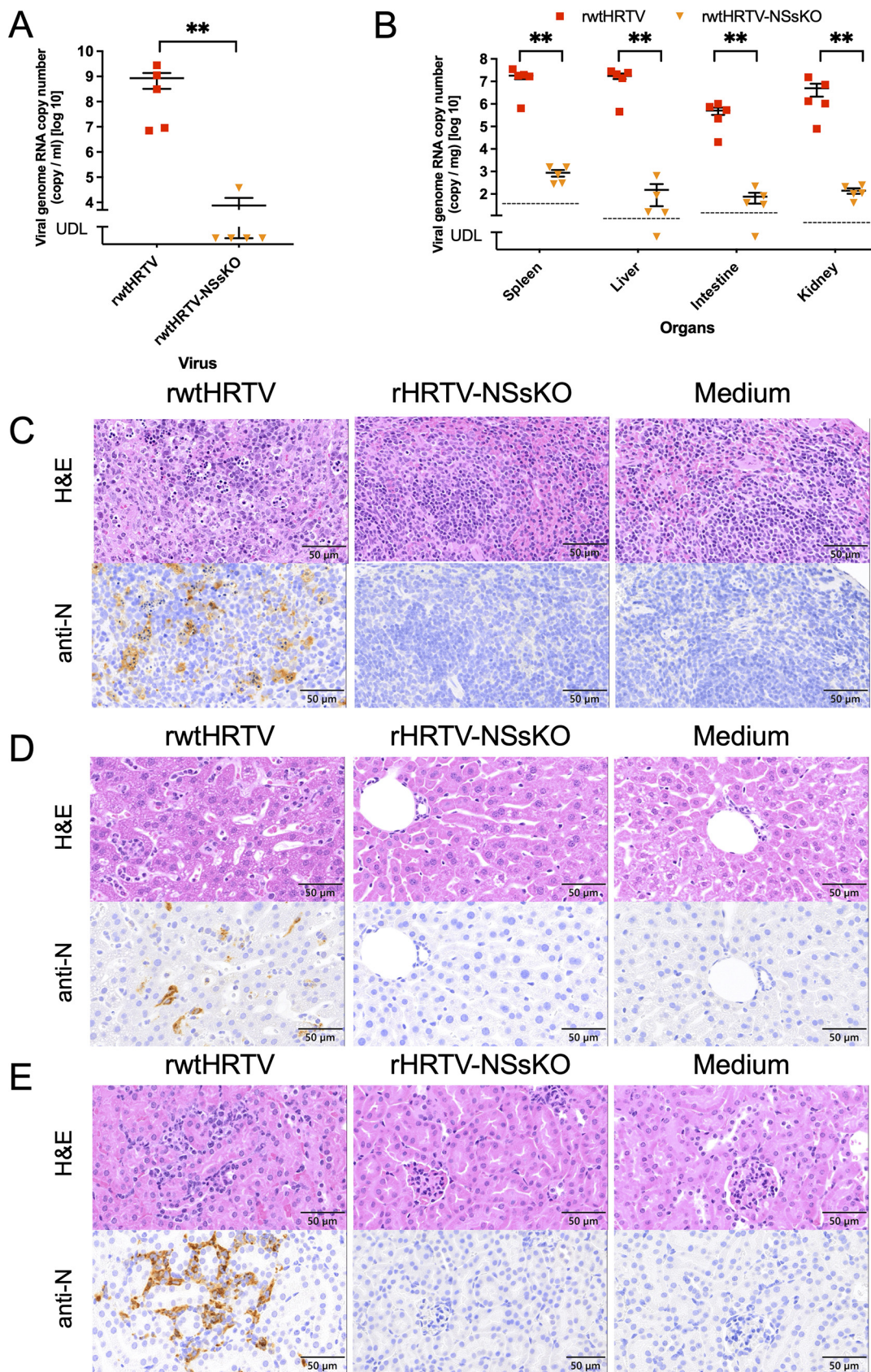


FIG 5 Comparison of the viral RNA loads in the plasma and each organ of mice infected with rwtHRTV or rHRTV-NSsKO. AG129 mice ($n = 5/\text{group}$) were infected with 1.0×10^2 FFU of rwtHRTV or rHRTV-NSsKO. On 7 dpi, mice were euthanized, (Continued on next page)

(Table 2). Thus, viral RNAs were supplied using RNA polymerase I, whereas N and L proteins were supplied using T7 RNA polymerase.

Bunyaviruses propagate in the cytoplasm of infected cells. Proteins expressed by the T7 RNA polymerase are transcribed in the cytoplasm, whereas proteins expressed by RNA polymerase II are transcribed in the nucleus (25). This difference may affect the success of the reverse genetics system for HRTV. A Rift Valley fever virus (RVFV; family *Phenuiviridae*) reverse genetics system in which L protein was supplied by RNA polymerase II was reported previously (25). We are unable to explain why reverse genetics succeeds for RVFV but not for HRTV in the presence of the L protein produced through RNA polymerase II activity, as shown here. Their virus-specific subcellular localizations, such as the L protein or its expression level in infected cells, may determine whether the viruses are rescued. Recently, an SFTSV reverse genetics system employing an RNA polymerase II-driven L protein was reported (26). Further research is therefore required to determine why, in the present study, the HRTV reverse genetics cannot work under the supplies of the L protein by RNA polymerase II.

The replication competencies of authentic isolated virus wtHRTV and the recombinant virus rwtHRTV were similar with slight differences (Fig. 3B). The authentic isolated virus comprises quasispecies, whereas the recombinant virus was derived from monoclonal plasmids. Moreover, one amino acid sequence difference was identified in the L proteins of wtHRTV and rwtHRTV (G86E). These differences may slightly affect virus replication.

Several recent reports suggest that SFTSV NSs inhibits the induction of type I IFN and facilitates disease progression (16, 18, 19, 27, 28). HRTV NSs has been considered to act as an antagonist of type I IFN, as indicated by the results of NSs transient expression studies (17–20). However, it is unclear whether NSs acts as a type I IFN antagonist in HRTV-infected cells. We verified it using the reverse genetics system for the HRTV developed here.

The plaque morphology of rHRTV-NSsKO in Vero 9013 cells was unclear (Fig. 4C). Furthermore, the growth capacity of rHRTV-NSsKO in Vero 9013 cells, which do not express type I IFN, was $>10^2$ times lower than that of rwtHRTV at 96 h postinfection (Fig. 4D). It has been reported that the growth capacity of the NSs gene mutated in SFTSV in Vero cells is similar to that of SFTSV (23). The growth of rHRTV-NSsKO in A549 cells, which express type I IFN, was reduced drastically compared with that of rwtHRTV (Fig. 4E). These results suggest that HRTV NSs not only blocked type I IFN induction but also were involved in other innate immune systems, which were functional in Vero 9013 cells. Further studies are needed to confirm this hypothesis.

The levels of type I IFN-related mRNAs in rHRTV-NSsKO-infected A549 cells detected here support the previously reported hypothesis related to transient NSs expression (Fig. 4F to H) (17–20). The results suggest that the HRTV NSs gene knockout induced the expression of IFN- β . The induction of ISGs was detected in cells infected with rHRTV-NSsKO (Fig. 4G, H, and K). These results supported the conclusion that NSs inhibited type I IFN signaling. Furthermore, the results of the transient expression of NSs in 293T cells support these results and the results reported previously by Rezeli et al. (Fig. 4L and M) (17).

HRTV NSs gene knockout induced the expression of RIG-I and TLR3 in infected cells (Fig. 4I and J), suggesting that NSs inhibited the induction of type I IFN as well as genes that encode upstream components of signaling pathways that regulate innate immunity. For example, abrogation of TLR3 expression leads to evasion of the recognition of viruses with double-stranded RNA (dsRNA) genomes (29). We show here that the level

FIG 5 Legend (Continued)

and plasma and organ samples were collected. (A and B) RNAs were extracted, and viral RNA loads in plasma and organs were determined using qRT-PCR. (C, D, and E) Hematoxylin and eosin (H&E) staining and IHC analysis using an anti-N antibody were performed on spleen (C), liver (D), and kidney samples (E). UDL, under detection limit. Error bars in A and B represent the SEM. **, $P < 0.01$. Dashed lines in B represent detection limits. The scale bars in C, D, and E represent 50 μm .

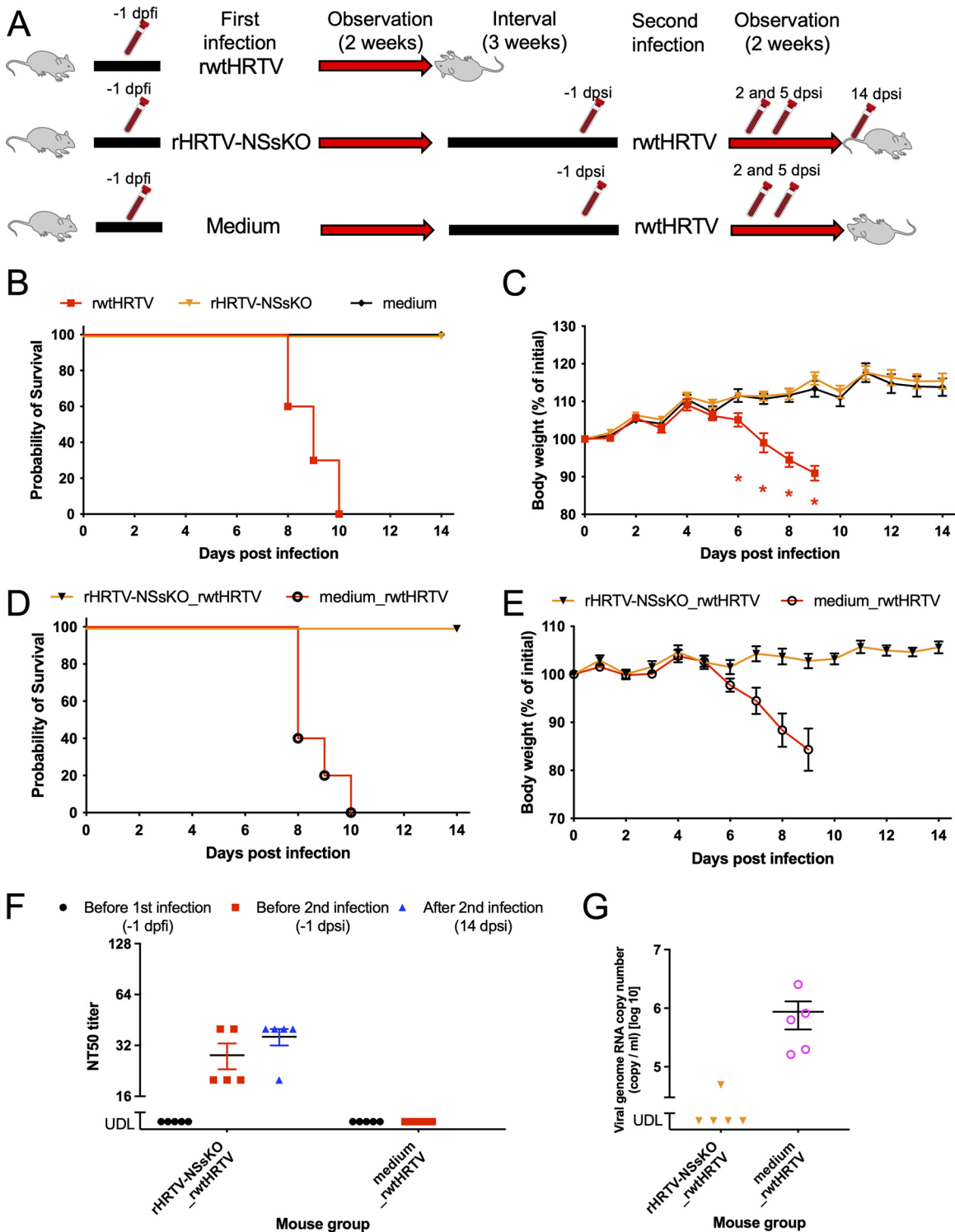


FIG 6 Virulence of rHRTV-NSsKO in AG129 mice and the potential of the viruses to develop anti-HRTV live-attenuated vaccines. (A) Diagram of the protocols. Mice ($n = 10/\text{group}$) were infected with 1.0×10^2 FFU of recombinant viruses denoted in the column labeled "first infection" and were observed for 2 weeks. Five weeks after the first infection, half of survivors ($n = 5/\text{group}$) were further infected with 1.0×10^2 FFU of rwtHRTV. Blood collection tubes in the diagram indicate the collection of blood samples, which were collected -1 day post-first infection (dpfi) and $-1, 2, 5,$ and 14 days post-second infection (dpi). (B) Survival curves of the first infection experiment. $P < 0.001$ (rwtHRTV versus rHRTV-NSsKO). (C) Body weight changes of infected mice of the first infection experiment performed in B. (D) Survival curves of the second infection experiment performed in B. (E) Body weight changes of infected mice in the second infection experiment performed in D. (F) Kinetics of neutralization titers against HRTV in infected mice. NT₅₀ values of plasma samples collected -1 days before first infection (dpfi), -1 (before second infection), and 14 days post-second infection (dpi). (G) HRTV viral RNA loads in plasma samples collected 5 dpi. Error bars in C, E, F, and G represent the SEM. *, $q < 0.05$ (rwtHRTV versus rHRTV-NSsKO). UDL, under detection limit.

of TLR3 mRNA in rwtHRTV-infected cells was the same as that in uninfected cells. In contrast, the level of TLR3 mRNA in rHRTV-NSsKO-infected cells was approximately 40-fold higher in comparison (Fig. 4J). These results suggest that NSs is required for authentic HRTV to evade the host immune system by escaping recognition by TLR3.

The effects of bandavirus NSs on the downstream components of the TLR3 and RIG-I pathways are well studied (28, 30). For example, SFTSV NSs sequesters TANK-binding kinase 1 (TBK1) into NSs-induced cytoplasmic structures to inhibit the phosphorylation and nuclear translocation of IFN regulatory factor 3 (IRF3) and subsequent IFN- β production (30). HRTV NSs inhibits TBK1-IRF3 signaling by not sequestering TBK1 into NSs-induced cytoplasmic structures. In contrast, HRTV NSs interacts directly with TBK1 and impedes the interaction between TBK1 and IRF3 (18). TBK1-IRF3 signaling occurs downstream of the TLR3 and RIG-I pathways. Further studies are therefore required to identify the roles of NSs in infected cells.

AG129 mice were reported previously to be susceptible to HRTV infection (31). rHRTV-NSsKO was less pathogenic than rwtHRTV (Fig. 5). Moreover, the lethality of rHRTV-NSsKO in mice was 0% (Fig. 6B). AG129 mice lack type I and II IFN receptors (IFN $\alpha\beta\gamma$ R $^{-/-}$). In this regard, we are unable to explain the reduction of the pathogenicity of rHRTV-NSsKO for AG129 mice. In SFTSV, it is reported that NSs activated the tumor progression locus 2 (TPL2) signaling pathway. This activation resulted in the marked upregulation of IL-10 expression, which dampened the host defense and promoted viral pathogenesis (23). However, further studies should investigate whether HRTV NSs in the TPL2 signaling pathway affects the pathogenicity of HRTV in AG129 mice.

Recently, it was reported that domestic cats were susceptible to SFTSV, with a fatality rate of 62.5% (32). However, the prevalence of HRTV in domestic animals and their susceptibility to HRTV are unknown. Furthermore, the number of known human cases affected by the HRTV disease is currently limited, and hence, vaccine development against HRTV is not urgent (3). Nevertheless, preparing an HRTV vaccine for humans and animals is important for public health. Modifying the NSs gene is one of the attenuation strategies employed to develop an RVFV vaccine (33). The results of secondary infection of rHRTV-NSsKO-infected mice demonstrated the vaccine potency of NSs gene-knockout HRTV (Fig. 6A and D). Notably, all mice inoculated with rHRTV-NSsKO survived after infection with a lethal dose of rwtHRTV, and 80% of these mice did not show viremia after infection (Fig. 6G). Therefore, rHRTV-NSsKO may serve as a live-attenuated vaccine against HRTV. Anti-HRTV neutralizing antibodies were induced in mice infected with rHRTV-NSsKO after the first infection (Fig. 6F). As observed, the induction level of anti-HRTV neutralizing antibodies after the 2nd infection was virtually equal to that after the 1st infection, suggesting that humoral and cellular immunity are deeply involved in protecting against HRTV infections. Nevertheless, the role of cellular immunity against HRTV infection is unclear. Hence, further studies should elucidate how cellular immunity contributes to antiviral responses during HRTV infections.

In summary, here, we have developed the reverse genetics system for HRTV and have analyzed the function of NSs and the pathogenic effects of HRTV. The effect of NSs gene knockout was analyzed, and the vaccine potency of NSs gene-knockout HRTV (rHRTV-NSsKO) was assessed in mice. The results suggest that rHRTV-NSsKO may serve as a live-attenuated vaccine against HRTV infection. Further studies using the HRTV reverse genetics system established in this study would help in the development of vaccines and the analyses of HRTV pathogenesis.

MATERIALS AND METHODS

Cells and viruses. African green monkey kidney Vero cells (strain 9013) (Vero 9013 cells) were cultured at 37°C in an atmosphere containing 5% CO₂ in Eagle's minimal essential medium (MEM) (Sigma-Aldrich, St. Louis, MO) supplemented with 5% heat-inactivated fetal bovine serum (FBS) (Sigma-Aldrich) and 100 μ g/mL penicillin-streptomycin (Nacalai tesque, Kyoto, Japan). A549 and 293T cells were maintained in Dulbecco's modified Eagle medium (DMEM) (Sigma-Aldrich), supplemented with 10% FBS and 100 μ g/mL penicillin-streptomycin (DMEM-10FBS), and cultured at 37°C in 5% CO₂. BSR-T7/5 cells (provided by Karl-Klaus Conzelmann) were maintained in Glasgow's MEM (G-MEM) (Nacalai tesque) supplemented with 10% FBS, 10% tryptose phosphate broth (Thermo Fisher Scientific, Carlsbad, CA), 100 μ g/

mL penicillin-streptomycin, and 1 mg/mL of G418 (Thermo Fisher Scientific), every other passage (G-MEM-10FBS) and cultured at 37°C in 5% CO₂ (34).

HRTV strain MO-4 (provided by Robert B. Tesh, University of Texas Medical Branch, Galveston, TX) was passaged four times in Vero cells, and viral sequences were determined as described below (HRTV strain MO-4-NIID). HRTV strain MO-4-NIID passaged in Vero 9013 cells served as wtHRTV.

Plasmids. To construct the plasmids designated pRF-HRTV-S, pRF-HRTV-M, and pRF-HRTV-L, cDNA fragments containing complete S, M, or L segments of HRTV were cloned between the sequences encoding the murine pol I promoter and the terminator of the pRF vector (35). The pRF vector system was provided by Shuzo Urata, Nagasaki University (Nagasaki, Japan), and Juan Carlos de la Torre, the Scripps Research Institute (San Diego, CA). Viral cDNA constructs were inserted in the genomic sense orientation of the viral RNA (vRNA). The pRF-HRTV-S plasmid with mutations in the ORF of the NSs gene (pRF-HRTV-S-mutaNSs) was generated via site-directed mutagenesis and an in-fusion high-fidelity (HD) restriction-free cloning method (TaKaRa Bio, Shiga, Japan). Plasmids for the expression of HRTV N and HRTV L (referred to as pTM1-HRTV-N and pTM1-HRTV-L, respectively) were constructed by cloning PCR amplicons of the HRTV N and HRTV L genes, which were inserted into an EcoRI-linearized pTM1 plasmid using an in-fusion HD restriction-free cloning method. The pTM1 plasmid is a T7-driven expression plasmid, and an internal ribosome entry site (IRES) is present between the T7 promoter and protein ORF sequences. Plasmids for the expression of HRTV N and HRTV L (referred to as pKS-HRTV-N and pKS-HRTV-L, respectively) were constructed by cloning PCR amplicons of the HRTV N and HRTV L genes into EcoRI-linearized pKS336 plasmid by an in-fusion HD restriction-free cloning method. Plasmid for the expression of HRTV NSs tagged with the *c-myc*-tag at the C terminus (referred to as pKS-HRTV-NSs-*c-myc*) was constructed by cloning the PCR amplicon of the HRTV NSs gene linked to the *c-myc* tag gene into a BamHI-linearized pKS336 plasmid using an in-fusion HD restriction-free cloning method. A plasmid expressing *Renilla* luciferase (Rluc) (referred to as pRL-TK) was purchased from Promega (Fitchburg, WI). A plasmid expressing firefly luciferase (Fluc) (referred to as pT7-Fluc) was provided by Yoshiharu Matsuura, Osaka University (Osaka, Japan). The plasmids pSRE-TA-luc and pTA-luc plasmids were purchased from TaKaRa Bio.

Minigenome assay. Eighty microliters of BSR-T7/5 cells (2.0×10^5 /mL) were seeded into the wells of a 96-well black/clear flat bottom tissue culture (TC)-treated imaging microplate (Corning, Corning, NY) and grown to approximately 80% confluence. Cells were transfected with minigenome plasmids (1.0×10^{-1} μ g of HRTV-MMG), 5.0×10^{-2} μ g of pTM1-HRTV-N (or pKS-HRTV-N) or pCAGGS vector (empty vector), 1.0×10^{-2} μ g of pTM1-HRTV-L (or pKS-HRTV-L) or empty vector, and 5.0×10^{-3} μ g of pT7-Fluc. Transfections were conducted in the presence of a TansIT-LT1 DNA transfection reagent (Mirus Bio, Madison, WI). Cells were transfected with 0.165 μ g (0.33 μ L) of total plasmids. Transfected cells were incubated for 2 days at 37°C. Nluc and Fluc activities were measured using a Nano-Glo dual-luciferase reporter assay system (Promega, Fitchburg, WI). Luminescence was measured, and the relative light units (RLUs) of luciferase were determined using a Wallac Victor 3V luminometer (PerkinElmer, Waltham, MA). All results obtained for Nluc were normalized to the expression levels of Fluc.

Reverse genetics assay. Four milliliters of BSR-T7/5 cells (2.0×10^5 /mL) were added to 50-mm-diameter dishes and cultured to approximately 80% confluence. Cells were transfected using 14.4 μ L of a TansIT-LT1 DNA transfection reagent with 2.0 μ g of pRF-HRTV-S (or mutated pRF-HRTV-S; pRF-HRTV-S-mutaNSs), 2.0 μ g pRF-HRTV-M, 2.0 μ g of pRF-HRTV-L, 1.0 μ g of pTM1-HRTV-N (or pKS-HRTV-N), and 2.0×10^{-1} μ g of pTM1-HRTV-L (or pKS-HRTV-L). Cells were incubated for at least 2 days at 37°C. The medium used for culturing BSR-T7/5 cells (supernatant) was removed and then added to Vero 9013 cells and incubated for 7 days. After viral propagation was confirmed using an immunofocus assay, the supernatants were further passaged in Vero cells and incubated for at least 4 days. The supernatants were harvested and stored at -80°C . The RNA of each recombinant virus was extracted, and the viral genome sequences of all recombinant viruses were confirmed using Sanger sequencing (36).

Viral genome sequencing. Viral genome sequences of all HRTVs used here were analyzed using Sanger sequencing of viral cDNAs generated using reverse transcription-PCR (RT-PCR). To determine the 3' terminus of the viral genome sequence, total RNA was extracted from infected Vero 9013 cells and polyadenylated *in vitro* using a poly(A) tailing kit (Thermo Fisher Scientific, Carlsbad, CA), according to the manufacturer's instructions. Samples were subsequently purified using an RNeasy minikit (Qiagen, Venlo, Netherlands). Purified polyadenylated RNA was used as the template for a one-step RT-PCR with an oligo(dT)-containing adaptor primer and gene-specific primer (GSP). PCR products were subsequently subjected to a second PCR amplification using the rapid amplification of cDNA ends (RACE) primer and GSPs. A 5' RACE system (Thermo Fisher Scientific) was used to determine the sequence of the 5' terminus of the viral genome sequence. Briefly, cDNAs were synthesized from RNAs using GSPs and tailed with homopolymeric dCTP (55083; Thermo Fisher Scientific). Then cDNAs were treated with terminal deoxynucleotidyl transferase (Thermo Fisher Scientific) and subjected to PCRs with GSPs, abridged anchor primer, and universal amplification primer. All these PCR products were purified, and their nucleic sequences were analyzed by Sanger sequencing (36).

Antibodies. A polyclonal antibody raised against the HRTV recombinant N protein (rabbit anti-N) was produced in the present study. The HRTV recombinant N protein tagged with a histidine-tag at the C terminus was expressed in a baculovirus expression system as described previously (9). Anti-N protein sera were raised in rabbits by immunization with purified HRTV-N (rabbit anti-N). A polyclonal antibody raised against the SFTSV NSs protein (rabbit anti-NSs) was provided by Hiroki Kato, Kyoto University (Kyoto, Japan). The cross-reactivity of rabbit anti-NSs against HRTV NSs was confirmed, and rabbit anti-NSs was used to detect HRTV NSs. A monoclonal antibody against α -tubulin (T5168; Sigma-Aldrich) and a polyclonal antibody against *c-myc* (C3956; Sigma-Aldrich) served as primary antibodies in Western blot assays.

Immunofocus, immunofluorescence (IFA), and plaque formation assays. The infectious dose of HRTV was determined using a viral immunofocus assay. Briefly, after 1-h adsorption of virus solution to Vero 9013 cells cultured in 12-well plates, cells were overlaid with 1 mL of maintenance medium (Eagle's MEM containing 1% methylcellulose, 2 mM L-glutamine, 0.22% sodium bicarbonate, and 2% FBS) and further cultured for 7 days at 37°C. The cell monolayers were then fixed with 10% formalin in phosphate-buffered saline (PBS), permeabilized using 0.2% Triton X-100 in PBS, and reacted with rabbit anti-N and horseradish peroxidase (HRP)-goat anti-rabbit IgG (H+L) DS Grd (917439A; Life Technologies). Cells were then stained using a peroxidase stain oxidized by hydrogen peroxide (DAB) kit (Nacalai tesque), and the number of stained foci was counted. The immunofluorescence assay (IFA) employed Alexa Fluor 488 goat anti-rabbit IgG (H+L) (Life Technologies) as the secondary antibody. The cells were observed to detect HRTV using a fluorescence microscope (BZ-9000; Keyence, Osaka, Japan). In the plaque formation assay, fixed cells were stained using methylene blue, washed with tap water, and dried.

Comparison of viral growth kinetics of authentic and recombinant viruses. The viral growth kinetics of authentic virus and the recombinant virus (wtHRTV versus rwtHRTV) in Vero 9013 cells were analyzed. Briefly, confluent monolayers of Vero 9013 cells cultured in 12-well plates were infected with each virus at a multiplicity of infection (MOI) of 0.1. Cells were washed three times with MEM supplemented with 2% FBS (MEM-2FBS) after a 1-h adsorption period at 37°C, and 1 mL of MEM-2FBS was added to each well. Supernatant samples were collected at 0, 24, 48, 72, and 96 h postinfection. The supernatants were centrifuged at $8,000 \times g$ for 2 min to remove cell debris and were stored at -80°C until the infectious dose was measured using a viral immunofocus assay. Virus growth curves were generated using GraphPad Prism 7 software and analyzed using Welch's *t* test at each sampling time.

Comparison of viral growth kinetics of WT and NSs-KO viruses. The growth kinetics of recombinant the wt virus and NSs-KO virus (rwtHRTV versus rHRTV-NSsKO) in Vero 9013 and A549 cells were analyzed. Briefly, confluent monolayers of Vero 9013 and A549 cells cultured in 12-well plates were infected with each virus at an MOI of 0.01 per cell. Cells were washed three times with MEM-2FBS (Vero 9013 cells) or DMEM supplemented with 2% FBS (DMEM-2FBS) (A549 cells) after a 1-h adsorption period at 37°C, and 1 mL of MEM-2FBS or DMEM-2FBS was added to each well. Supernatant samples were collected at 0, 24, 48, 72, and 96 h postinfection. The supernatants were centrifuged at $8,000 \times g$ for 2 min to remove cell debris and were stored at -80°C until the infectious dose was measured using a viral immunofocus assay. Virus growth curves were generated using GraphPad Prism 7 software and analyzed using Welch's *t* test at each sampling time. Infected and uninfected A549 cells were harvested 24 h postinfection, and RNA was extracted using the TRIzol reagent (Thermo Fisher Scientific).

IFN- β and ISRE reporter assays. For the transient NSs expression assay, 100 μL of $2.0 \times 10^5/\text{mL}$ 293T cells were added to a 96-well black/clear flat-bottom TC-treated imaging microplate and cultured to approximately 80% confluence. The cells were transfected using the TansIT-LT1 DNA transfection reagent with 20 ng pISRE-TA-luc or pTA-luc, 10 ng pRL-TK, and 10 ng pKS-HRTV-NSs-*c-myc* or pKS336 (empty vector). Cells were incubated for 48 h at 37°C in an atmosphere containing 5% CO_2 and then treated with 100 units of IFN- β (407318; Sigma-Aldrich). After 18 h, the activities of Fluc and Rluc were measured using a dual-luciferase reporter assay system (Promega). The expression levels of Rluc served to normalize the results obtained for Fluc.

For assays of the authentic virus, 100 μL of $2.0 \times 10^5/\text{mL}$ 293T cells were added to 96-well black/clear flat-bottom TC-treated imaging microplate and cultured to reach approximately 80% confluence. The cells were transfected using the TansIT-LT1 DNA transfection reagent with 20 ng pISRE-TA-luc or pTA-luc and 10 ng pRL-TK. Cells were incubated for 15 h at 37°C (5% CO_2) and then inoculated with recombinant viruses at an MOI of 2. After 48 h, the activities of Fluc and Rluc were measured using a dual-luciferase reporter assay system (Promega). The expression levels of Rluc served to normalize all the results obtained for Fluc. One-way analysis of variance (ANOVA) and Tukey's multiple-comparison test were used to analyze the RLU levels.

Quantitative RT-PCR (qRT-PCR) analysis of relative mRNA expression levels of host immune-related genes. Total RNA extracted from infected and uninfected A549 cells were reverse transcribed using ReverTra Ace quantitative PCR (qPCR) RT master mix with genomic DNA (gDNA) remover (Toyobo, Osaka, Japan). Thunderbird SYBR qPCR mix (Toyobo) and a QuantStudio 5 real-time PCR system (Thermo Fisher Scientific) were used for qRT-PCR with the primers listed in Table 3 (19, 23, 37). The relative mRNA levels of the indicated genes were analyzed using the threshold cycle ($2^{-\Delta\Delta\text{CT}}$) method using qRT-PCR (38). The C_T of GAPDH was used as internal reference. One-way ANOVA and Tukey's multiple-comparison test were used to analyze the mRNA expression levels.

Western blot analysis. Cell lysates (60 μL) were mixed with 20 μL of a 4 \times sample buffer solution containing 20 vol% 2-mercaptoethanol (191-13272; Wako, Osaka, Japan). Proteins were separated on a sodium dodecyl sulfate (SDS) 4% to 12% gradient polyacrylamide gel (Thermo Fisher Scientific, Carlsbad, CA). Proteins were transferred electrophoretically to a polyvinylidene difluoride membrane (Bio-Rad Laboratories, Hercules, CA), and the membrane was then blocked by incubating in saturation buffer (Tris-buffered saline [TBS] containing 0.25% skim milk and 0.05% Tween 20). The membrane was then incubated with the primary antibodies described above. After being washed with TBS containing 0.05% Tween 20, the membrane was incubated with the HRP-labeled secondary antibodies HRP-conjugated goat anti-rabbit IgG (H+L) DS Grd (31460; Life Technologies) or HRP-conjugated goat anti-mouse IgG (H+L) (62-6520; Thermo Fisher Scientific). Protein expression was detected using the Immobilon western chemiluminescent HRP substrate (Millipore, Burlington) according to the manufacturer's instructions. Bands were visualized using an LAS-3000 mini instrument (Fujifilm, Tokyo, Japan).

Mouse experiments. Animal experiments were performed in an animal biosafety level 3 laboratory. All experiments were performed following the Guidelines for Animal Experimentation of the NIID, Japan,

TABLE 3 List of real-time PCR primers and probes used in this study

Name	Primer or probe	Sequence	Target	Reference
HRTV4-forward	Primer	CCTTTGGTCCACATTGATTG	HRTV NSs	39
HRTV4-reverse	Primer	CACTGATTCCACAGGCAGAT	HRTV NSs	39
HRTV4-probe	Probe	FAM-TGGATGCCTATTCCTTTGGCAA-TAMRA ^a	HRTV NSs	39
human GAPDH-Fw	Primer	GAAGGTGAAGGTCGGAGTC	Human GAPDH	23
human GAPDH-Rv	Primer	GAAGATGGTGATGGGATTC	Human GAPDH	23
human IFN- β Fw	Primer	CTCCTGGCTAATGTCTATCA	Human IFN- β	19
human IFN- β Rv	Primer	GCAGAATCCTCCATAATAT	Human IFN- β	19
human ISG15-Fw	Primer	CGCAGATCACCCAGAAGATT	Human ISG15	37
human ISG15-Rv	Primer	GCCCTTGTTATTCCTCACCA	Human ISG15	37
human MxA-Fw	Primer	GTGCATTGCAGAAGGTCAGA	Human mxa	37
human MxA-Rv	Primer	CTGGTGATAGGCCATCAGGT	Human mxa	37
human RIG-I-Fw	Primer	CTTGGCATGTACACAGCTGAC	Human RIG-I	37
human RIG-I-Rv	Primer	GCTTGGGATGTGGTCTACTCA	Human RIG-I	37
human TLR3-Fw	Primer	TCCAAGCCTTCAACGACTG	Human TLR3	37
human TLR3-Rv	Primer	TGGTGAAGGAGAGCTATCCACA	Human TLR3	37

^aFAM, 6-carboxyfluorescein; TAMRA, 6-carboxytetramethylrhodamine.

which were approved by the Committee on Experimental Animals at NIID (numbers 119174 and 120079). Specific pathogen-free 4- to 5-week-old female AG129 mice were bred and used in the present study.

Replication kinetics of the NSs knockout virus in mice. Mice were infected s.c. with 1.0×10^2 FFU of rwtHRTV, rHRTV-NSsKO, or medium ($n = 5$ /group). Mice infected with rwtHRTV or rHRTV-NSsKO were euthanized using deep isoflurane anesthesia, and blood samples were collected by cardiac puncture at 7 dpi. Organ tissues were collected and immersed in TRIzol (Thermo Fisher Scientific) or 4% paraformaldehyde-phosphate buffer solution (Fujifilm, Tokyo, Japan). Blood samples were centrifuged, and plasma samples were collected.

Evaluation of the virulence of rHRTV-NSsKO in mice and its evaluation as vaccine candidates. Mice were infected s.c. with 1.0×10^2 FFU of rwtHRTV, rHRTV-NSsKO, or medium ($n = 10$ /group). Mice were monitored daily for 14 days for clinical symptoms, body weight, and survival. Mice with $>20\%$ weight loss were euthanized to avoid suffering to the extent possible. After the first infection, half of rHRTV-NSsKO- and medium-infected mice ($n = 5$ /group) were inoculated s.c. with 1.0×10^2 FFU of rwtHRTV 35 dpi (0 dpi) and monitored daily for 14 days for clinical symptoms, body weight, and survival. After 14 dpi, mice were euthanized using deep isoflurane anesthesia. Blood was collected from the caudal vein of each mouse on -1 dpi, -1 dpi, 2 dpi, and 5 dpi. Blood samples were collected in Microtainer blood collection tubes (BD, Franklin Lakes, NJ) and centrifuged at $8,000 \times g$ for 5 min. Separated plasma was stored at -80°C . We used GraphPad Prism 7 software to generate survival curves, which were analyzed using the log-rank (Mantel-Cox) test. The curves of body weight changes were generated using GraphPad Prism 7 software and those after the initial infection were analyzed using multiple t tests. Discovery was determined using two-stage linear step-up produced by Benjamini, Krieger, and Yekutieli, with a Q (the desired maximum percent of discoveries that are false discoveries) of 1% (35).

Analysis of viral genome copy number in mouse samples. Plasma samples were mixed with the binding buffer included in the high pure viral RNA purification kit (Roche Diagnostics, Indianapolis, IN) to extract RNA. Liver, spleen, kidney, and intestine samples were immersed immediately in 1 mL of TRIzol (Thermo Fisher Scientific) and stored at -80°C . Then, samples were thawed, and RNA was extracted according to the manufacturer's instructions. Viral genome copy numbers were determined using qRT-PCR as follows: the forward and reverse primers and probes for HRTV are listed in Table 3 (39). The qRT-PCR assays were performed using a QuantStudio 5 real-time PCR system (Thermo Fisher Scientific) with TaqMan fast virus 1-step master mix (Thermo Fisher Scientific). The qRT-PCR protocol was as follows: reverse transcription (48°C for 5 min), denaturation (95°C for 20 s), 40 cycles of amplification, and quantification (95°C for 3 s and 57°C for 30 s). In the present study, the standard control for HRTV was 10-fold serial dilutions of the RNAs containing the partial amplicons of the N genes of HRTV. These RNAs were synthesized using an *in vitro* transcription assay (40). Viral genome copy numbers were calculated as the ratio of the copy number of each standard control. Viral genome copy numbers were plotted using GraphPad Prism software, and the results were analyzed using the Mann-Whitney test. The viral RNA detection limits in the plasma, spleen, liver, intestine, and kidney were 2.5×10^3 copies/mL, 5.6×10^1 copies/mg, 1.5×10^1 copies/mg, 1.9×10^1 copies/mg, and 1.1×10^1 copies/mg, respectively.

Histopathology and immunohistochemistry (IHC). Tissue samples were immersed in 4% paraformaldehyde-phosphate buffer solution (Fujifilm, Tokyo, Japan) and fixed, and the fixed tissue specimens were embedded in paraffin. Tissue sections ($3 \mu\text{m}$) were cut and mounted onto glass slides for standard hematoxylin and eosin staining or IHC analysis of viral antigens. Rabbit anti-N was used as the primary antibody, and a peroxidase-labeled polymer-conjugated anti-rabbit immunoglobulin (EnVision/HRP; Dako) served as the secondary antibody. Immune complexes were visualized using 3,3'-diaminobenzidine tetrahydrochloride. Hematoxylin (modified Mayer's) was used as a nuclear counterstain in IHC. Histopathological and IHC images were acquired using a Slideview VS200 device (Olympus, Tokyo, Japan).

Neutralization assay. Heat-inactivated (56°C for 30 min) plasma was serially diluted 2-fold (1:20 to 1:640) with MEM-2FBS, and the diluted samples were mixed with an equal volume of MEM-2FBS containing 50 to 150 FFU/50 μ L wtHRTV. The mixtures were incubated for 1 h at 37°C. Vero cells cultured in 12-well plates were inoculated with 100 μ L of each mixture and cultured at 37°C for 1 h for adsorption. The cells were overlaid with 1 mL of maintenance medium (Eagle's MEM containing 1% methylcellulose, 2 mM L-glutamine, 0.22% sodium bicarbonate, and 2% FBS). The plates were incubated at 37°C (5% CO₂) for 7 days. Cells were fixed with 10% formaldehyde, permeabilized by incubation with PBS containing 0.2% Triton X-100 (Sigma-Aldrich, St. Louis, MO) and then stained with rabbit anti-N serum and HRP-goat anti-rabbit IgG (H+L) DS Grd (Life Technologies). The cells were then stained with a peroxidase stain DAB kit (Nacalai tesque). The number of stained foci was counted as described above, and the 50% focus reduction of neutralization titer (FRNT₅₀) was measured. The FRNT₅₀ titers were defined as the reciprocal of the serum dilution with a focus number of <50% of the control, and the foci in the control wells were inoculated with the mixture of plasma-free MEM-2FBS and MEM-2FBS containing 50 to 150 FFU/50 μ L of wtHRTV.

ACKNOWLEDGMENTS

We thank Juan Carlos de la Torre and Shuzo Urata for providing the pRF vector system; Robert B. Tesh for providing HRTV strain MO-4; Karl-Klaus Conzelmann for providing BSR-T7/5 cells; Hiroki Kato for providing the anti-NSs antibody; and Mina Ogawa, Momoko Ogata, Makiko Ikeda, Ken-ichi Shibasaki, and Naoko Katsuta for technical assistance.

This research was funded by grants-in-aid from the Japan Society for the Promotion of Science Kakenhi (grant numbers 18K14599 and 15K21645) and by grants-in-aid from the Japan Agency for Medical Research and Development (AMED) (grant numbers JP18fk0108002, JP19fk0108081, JP20fk0108081, JP21fk0108081, and JP21fk0108123).

REFERENCES

1. Brault AC, Savage HM, Duggal NK, Eisen RJ, Staples JE. 2018. Heartland virus epidemiology, vector association, and disease potential. *Viruses* 10: 498. <https://doi.org/10.3390/v10090498>.
2. McMullan LK, Folk SM, Kelly AJ, MacNeil A, Goldsmith CS, Metcalfe MG, Batten BC, Albarino CG, Zaki SR, Rollin PE, Nicholson WL, Nichol ST. 2012. A new phlebovirus associated with severe febrile illness in Missouri. *N Engl J Med* 367:834–841. <https://doi.org/10.1056/NEJMoa1203378>.
3. Centers for Disease Control and Prevention. 2020. Heartland virus diseases (Heartland). Centers for Disease Control and Prevention, National Center for Emerging and Zoonotic Infectious Diseases (NCEZID), Division of Vector-Borne Diseases (DVBD), Atlanta, GA. <https://www.cdc.gov/heartland-virus/index.html>.
4. Riemersma KK, Komar N. 2015. Heartland virus neutralizing antibodies in vertebrate wildlife, United States, 2009–2014. *Emerg Infect Dis* 21: 1830–1833. <https://doi.org/10.3201/eid2110.150380>.
5. Bosco-Lauth AM, Panella NA, Root JJ, Gidlewski T, Lash RR, Harmon JR, Burkhalter KL, Godsey MS, Savage HM, Nicholson WL, Komar N, Brault AC. 2015. Serological investigation of heartland virus (Bunyaviridae: Phlebovirus) exposure in wild and domestic animals adjacent to human case sites in Missouri 2012–2013. *Am J Trop Med Hyg* 92:1163–1167. <https://doi.org/10.4269/ajtmh.14-0702>.
6. Dupuis AP, Il, Prusinski MA, O'Connor C, Maffei JG, Ngo KA, Koetzner CA, Santoriello MP, Romano CL, Xu G, Ribbe F, Campbell SR, Rich SM, Backenson PB, Kramer LD, Ciota AT. 2021. Heartland virus transmission, Suffolk County, New York, USA. *Emerg Infect Dis* 27:3128–3132. <https://doi.org/10.3201/eid2712.211426>.
7. Liang M, Yu X, Li D. 2019. Rename the genus Banyangvirus and the species Huaiyangshan banyangvirus (Bunyavirales: Phenuiviridae). <https://ictv.global/ICTV/proposals/2019.015M.zip>. Accessed 17 May 2020.
8. Yu XJ, Liang MF, Zhang SY, Liu Y, Li JD, Sun YL, Zhang L, Zhang QF, Popov VL, Li C, Qu J, Li Q, Zhang YP, Hai R, Wu W, Wang Q, Zhan FX, Wang XJ, Kan B, Wang SW, Wan KL, Jing HQ, Lu JX, Yin WW, Zhou H, Guan XH, Liu JF, Bi ZQ, Liu GH, Ren J, Wang H, Zhao Z, Song JD, He JR, Wan T, Zhang JS, Fu XP, Sun LN, Dong XP, Feng ZJ, Yang WZ, Hong T, Zhang Y, Walker DH, Wang Y, Li DX. 2011. Fever with thrombocytopenia associated with a novel bunyavirus in China. *N Engl J Med* 364:1523–1532. <https://doi.org/10.1056/NEJMoa1010095>.
9. Takahashi T, Maeda K, Suzuki T, Ishido A, Shigeoka T, Tominaga T, Kamei T, Honda M, Ninomiya D, Sakai T, Senba T, Kaneyuki S, Sakaguchi S, Satoh A, Hosokawa T, Kawabe Y, Kurihara S, Izumikawa K, Kohno S, Azuma T, Suemori K, Yasukawa M, Mizutani T, Omatsu T, Katayama Y, Miyahara M, Ijuin M, Doi K, Okuda M, Umeki K, Saito T, Fukushima K, Nakajima K, Yoshikawa T, Tani H, Fukushi S, Fukuma A, Ogata M, Shimojima M, Nakajima N, Nagata N, Katano H, Fukumoto H, Sato Y, Hasegawa H, Yamagishi T, Oishi K, Kurane I, Morikawa S, Saijo M. 2014. The first identification and retrospective study of severe fever with thrombocytopenia syndrome in Japan. *J Infect Dis* 209:816–827. <https://doi.org/10.1093/infdis/jit603>.
10. Kim KH, Yi J, Kim G, Choi SJ, Jun KI, Kim NH, Choe PG, Kim NJ, Lee JK, Oh MD. 2013. Severe fever with thrombocytopenia syndrome, South Korea, 2012. *Emerg Infect Dis* 19:1892–1894. <https://doi.org/10.3201/eid1911.130792>.
11. Tran XC, Yun Y, Van An L, Kim SH, Thao NTP, Man PKC, Yoo JR, Heo ST, Cho NH, Lee KH. 2019. Endemic severe fever with thrombocytopenia syndrome, Vietnam. *Emerg Infect Dis* 25:1029–1031. <https://doi.org/10.3201/eid2505.181463>.
12. Li J, Li S, Yang L, Cao P, Lu J. 2021. Severe fever with thrombocytopenia syndrome virus: a highly lethal bunyavirus. *Crit Rev Microbiol* 47:112–125. <https://doi.org/10.1080/1040841X.2020.1847037>.
13. Lin TL, Ou SC, Maeda K, Shimoda H, Chan JP, Tu WC, Hsu WL, Chou CC. 2020. The first discovery of severe fever with thrombocytopenia syndrome virus in Taiwan. *Emerg Microbes Infect* 9:148–151. <https://doi.org/10.1080/22221751.2019.1710436>.
14. Walter CT, Barr JN. 2011. Recent advances in the molecular and cellular biology of bunyaviruses. *J Gen Virol* 92:2467–2484. <https://doi.org/10.1099/vir.0.035105-0>.
15. Kimura M, Egawa K, Ozawa T, Kishi H, Shimojima M, Taniguchi S, Fukushi S, Fujii H, Yamada H, Tan L, Sano K, Katano H, Suzuki T, Morikawa S, Saijo M, Tani H. 2021. Characterization of pseudotyped vesicular stomatitis virus bearing the heartland virus envelope glycoprotein. *Virology* 556: 124–132. <https://doi.org/10.1016/j.virol.2020.10.006>.
16. Chaudhary V, Zhang S, Yuen KS, Li C, Lui PY, Fung SY, Wang PH, Chan CP, Li D, Kok KH, Liang M, Jin DY. 2015. Suppression of type I and type III IFN signalling by NSs protein of severe fever with thrombocytopenia syndrome virus through inhibition of STAT1 phosphorylation and activation. *J Gen Virol* 96:3204–3211. <https://doi.org/10.1099/jgv.0.000280>.
17. Rezelj VV, Li P, Chaudhary V, Elliott RM, Jin DY, Brennan B. 2017. Differential antagonism of human innate immune responses by tick-borne phlebovirus nonstructural proteins. *mSphere* 2:e00234-17. <https://doi.org/10.1128/mSphere.00234-17>.
18. Ning YJ, Feng K, Min YQ, Deng F, Hu Z, Wang H. 2017. Heartland virus NSs protein disrupts host defenses by blocking the TBK1 kinase-IRF3

- transcription factor interaction and signaling required for interferon induction. *J Biol Chem* 292:16722–16733. <https://doi.org/10.1074/jbc.M117.805127>.
19. Moriyama M, Igarashi M, Koshiba T, Irie T, Takada A, Ichinohe T. 2018. Two conserved amino acids within the NSs of severe fever with thrombocytopenia syndrome phlebovirus are essential for anti-interferon activity. *J Virol* 92:e00706–18. <https://doi.org/10.1128/JVI.00706-18>.
 20. Feng K, Deng F, Hu Z, Wang H, Ning YJ. 2019. Heartland virus antagonizes type I and III interferon antiviral signaling by inhibiting phosphorylation and nuclear translocation of STAT2 and STAT1. *J Biol Chem* 294:9503–9517. <https://doi.org/10.1074/jbc.RA118.006563>.
 21. Brennan B, Li P, Zhang S, Li A, Liang M, Li D, Elliott RM. 2015. Reverse genetics system for severe fever with thrombocytopenia syndrome virus. *J Virol* 89:3026–3037. <https://doi.org/10.1128/JVI.03432-14>.
 22. Brennan B, Rezelj VV, Elliott RM. 2017. Mapping of transcription termination within the S segment of SFTS phlebovirus facilitated generation of NSs deletant viruses. *J Virol* 91:e00743-17. <https://doi.org/10.1128/JVI.00743-17>.
 23. Choi Y, Park SJ, Sun Y, Yoo JS, Pudupakam RS, Foo SS, Shin WJ, Chen SB, Tschlis PN, Lee WJ, Lee JS, Li W, Brennan B, Choi YK, Jung JU. 2019. Severe fever with thrombocytopenia syndrome phlebovirus non-structural protein activates TPL2 signalling pathway for viral immunopathogenesis. *Nat Microbiol* 4:429–437. <https://doi.org/10.1038/s41564-018-0329-x>.
 24. Choi Y, Jiang Z, Shin WJ, Jung JU. 2020. Severe fever with thrombocytopenia syndrome virus NSs interacts with TRIM21 to activate the p62-Keap1-Nrf2 pathway. *J Virol* 94:e01684-19. <https://doi.org/10.1128/JVI.01684-19>.
 25. Habjan M, Penski N, Spiegel M, Weber F. 2008. T7 RNA polymerase-dependent and -independent systems for cDNA-based rescue of Rift Valley fever virus. *J Gen Virol* 89:2157–2166. <https://doi.org/10.1099/vir.0.2008/002097-0>.
 26. Xu M, Wang B, Deng F, Wang H, Wang M, Hu Z, Liu J. 2021. Establishment of a reverse genetic system of severe fever with thrombocytopenia syndrome virus based on a C4 strain. *Virol Sin* 36:958–967. <https://doi.org/10.1007/s12250-021-00359-x>.
 27. Qu B, Qi X, Wu X, Liang M, Li C, Cardona CJ, Xu W, Tang F, Li Z, Wu B, Powell K, Wegner M, Li D, Xing Z. 2012. Suppression of the interferon and NF-kappaB responses by severe fever with thrombocytopenia syndrome virus. *J Virol* 86:8388–8401. <https://doi.org/10.1128/JVI.00612-12>.
 28. Santiago FW, Covalada LM, Sanchez-Aparicio MT, Silvas JA, Diaz-Vizarreta AC, Patel JR, Popov V, Yu XJ, Garcia-Sastre A, Aguilar PV. 2014. Hijacking of RIG-I signaling proteins into virus-induced cytoplasmic structures correlates with the inhibition of type I interferon responses. *J Virol* 88:4572–4585. <https://doi.org/10.1128/JVI.03021-13>.
 29. Wu W, Zhang W, Duggan ES, Booth JL, Zou MH, Metcalf JP. 2015. RIG-I and TLR3 are both required for maximum interferon induction by influenza virus in human lung alveolar epithelial cells. *Virology* 482:181–188. <https://doi.org/10.1016/j.virol.2015.03.048>.
 30. Ning YJ, Wang M, Deng M, Shen S, Liu W, Cao WC, Deng F, Wang YY, Hu Z, Wang H. 2014. Viral suppression of innate immunity via spatial isolation of TBK1/IKKepsilon from mitochondrial antiviral platform. *J Mol Cell Biol* 6:324–337. <https://doi.org/10.1093/jmcb/mju015>.
 31. Bosco-Lauth AM, Calvert AE, Root JJ, Gidlewski T, Bird BH, Bowen RA, Muehlenbachs A, Zaki SR, Brault AC. 2016. Vertebrate host susceptibility to Heartland virus. *Emerg Infect Dis* 22:2070–2077. <https://doi.org/10.3201/eid2212.160472>.
 32. Matsuu A, Momoi Y, Nishiguchi A, Noguchi K, Yabuki M, Hamakubo E, Take M, Maeda K. 2019. Natural severe fever with thrombocytopenia syndrome virus infection in domestic cats in Japan. *Vet Microbiol* 236:108346. <https://doi.org/10.1016/j.vetmic.2019.06.019>.
 33. Smith DR, Johnston SC, Piper A, Botto M, Donnelly G, Shamblin J, Albarino CG, Hensley LE, Schmaljohn C, Nichol ST, Bird BH. 2018. Attenuation and efficacy of live-attenuated Rift Valley fever virus vaccine candidates in non-human primates. *PLoS Negl Trop Dis* 12:e0006474. <https://doi.org/10.1371/journal.pntd.0006474>.
 34. Buchholz UJ, Finke S, Conzelmann KK. 1999. Generation of bovine respiratory syncytial virus (BRSV) from cDNA: BRSV NS2 is not essential for virus replication in tissue culture, and the human RSV leader region acts as a functional BRSV genome promoter. *J Virol* 73:251–259. <https://doi.org/10.1128/JVI.73.1.251-259.1999>.
 35. Taniguchi S, Yoshikawa T, Shimojima M, Fukushi S, Kurosu T, Tani H, Fukuma A, Kato F, Nakayama E, Maeki T, Tajima S, Lim CK, Ebihara H, Kyuwa S, Morikawa S, Saijo M. 2020. Analysis of the function of the lymphocytic choriomeningitis virus S segment untranslated region on growth capacity in vitro and on virulence in vivo. *Viruses* 12:896. <https://doi.org/10.3390/v12080896>.
 36. Sanger F, Nicklen S, Coulson AR. 1977. DNA sequencing with chain-terminating inhibitors. *Proc Natl Acad Sci U S A* 74:5463–5467. <https://doi.org/10.1073/pnas.74.12.5463>.
 37. Chen X, Ye H, Li S, Jiao B, Wu J, Zeng P, Chen L. 2017. Severe fever with thrombocytopenia syndrome virus inhibits exogenous Type I IFN signaling pathway through its NSs invitro. *PLoS One* 12:e0172744. <https://doi.org/10.1371/journal.pone.0172744>.
 38. Schmittgen TD, Livak KJ. 2008. Analyzing real-time PCR data by the comparative C(T) method. *Nat Protoc* 3:1101–1108. <https://doi.org/10.1038/nprot.2008.73>.
 39. Savage HM, Godsey MS, Jr., Lambert A, Panella NA, Burkhalter KL, Harmon JR, Lash RR, Ashley DC, Nicholson WL. 2013. First detection of heartland virus (Bunyaviridae: Phlebovirus) from field collected arthropods. *Am J Trop Med Hyg* 89:445–452. <https://doi.org/10.4269/ajtmh.13-0209>.
 40. Yoshikawa T, Fukushi S, Tani H, Fukuma A, Taniguchi S, Toda S, Shimazu Y, Yano K, Morimitsu T, Ando K, Yoshikawa A, Kan M, Kato N, Motoya T, Kuzuguchi T, Nishino Y, Osako H, Yumishashi T, Kida K, Suzuki F, Takimoto H, Kitamoto H, Maeda K, Takahashi T, Yamagishi T, Oishi K, Morikawa S, Saijo M, Shimojima M. 2014. Sensitive and specific PCR systems for detection of both Chinese and Japanese severe fever with thrombocytopenia syndrome virus strains and prediction of patient survival based on viral load. *J Clin Microbiol* 52:3325–3333. <https://doi.org/10.1128/JCM.00742-14>.